Chemico-Biological Interactions 183 (2010) 349–356

Contents lists available at ScienceDirect

Chemico-Biological Interactions

journal homepage: www.elsevier.com/locate/chembioint

DNA binding and photocleavage properties and apoptosis-inducing activities of a ruthenium porphyrin complex [(Py-3′)TPP-Ru(phen)$_2$Cl]Cl and its heterometallic derivatives

Yanan Liu[a], Tianfeng Chen[a,b], Yum-Shing Wong[b], Wen-Jie Mei[a,c], Xiao-Mei Huang[c], Fang Yang[a], Jie Liu[a,*], Wen-Jie Zheng[a,*]

[a] Department of Chemistry, Jinan University, Guangzhou 510632, PR China
[b] Department of Biology, The Chinese University of Hong Kong, Hong Kong, PR China
[c] School of Pharmacy, Guangdong Pharmaceutical University, Guangzhou 510006, PR China

ARTICLE INFO

Article history:
Received 30 September 2009
Received in revised form
22 November 2009
Accepted 24 November 2009
Available online 1 December 2009

Keywords:
Ruthenium porphyrin complex
DNA-binding
Photocleavage
Apoptosis
Mitochondria

ABSTRACT

The interactions of a ruthenium porphyrin complex [(Py-3′)TPP-Ru(phen)$_2$Cl]Cl (phen = 1,10-phenanthroline, (Py-3′)TPP = 5-(3′-pyridyl-10,15,20-triphenylporphyrin) (**1**) and its heterometallic derivatives, [Ni(Py-3′)TPP-Ru(phen)$_2$Cl][PF$_6$] (**2**) and [Cu(Py-3′)TPP-Ru(phen)$_2$Cl][PF$_6$] (**3**), with calf thymus DNA have been investigated by spectroscopic and viscosity measurements in this study. The results showed that these synthetic complexes can bind to double strand helix DNA in groove binding mode, and the intrinsic binding constants of complexes **1**, **2** and **3**, as calculated according to the decay of the Soret absorption, are $(1.35 \pm 0.5) \times 10^5\ M^{-1}$ ($s = 4.2$), $(1.29 \pm 0.5) \times 10^5\ M^{-1}$ ($s = 5.6$) and $(1.22 \pm 0.5) \times 10^5\ M^{-1}$ ($s = 6.2$) (s is the binding-site size), respectively, which are consistent with those obtained from ethidium bromide-quenching experiments. Further investigations on the photocleavage properties of these complexes on plasmid pBR 322 DNA showed that complexes **1**, **2** and **3** could cleave single chain DNA and convert DNA molecules from supercoiled form to the nicked form. As determined by MTT assay, the complexes were also identified as potent antiproliferative agents against A375 human melanoma cells, MCF-7 human breast adrenocarcinoma cells, Colo201 human colon adenocarcinoma cells and HepG2 human liver cancer cells. Complex **1** inhibits the growth of A375 cells through induction of apoptotic cell death and G0/G1 cell cycle arrest. Further investigation on intracellular mechanisms indicated that Complex **1** induced depletion of mitochondrial membrane potential ($\Delta\Psi_m$) in A375 cells through regulating the expression of pro-survival and pro-apoptotic Bcl-2 family members. Our results suggest that ruthenium porphyrin complexes could be candidates for further evaluation as chemopreventive and chemotherapeutic agents for human cancers.

1. Introduction

Porphyrins and their metalloporphyrins have been widely studied due to their spectroscopic and electrochemical properties, and novel biological activities. Ruthenium (Ru), a rare transition metal of the platinum group, possesses several favorable properties suited to rational anticancer drug design, such as the higher coordination number by comparing with platinum, which could provide additional coordination sites that could potentially be used to fine-tune the properties of the complexes [1]. Ru porphyrin complexes have attracted much attention over the last decade due to their application potential as anticancer drugs [1–5] and novel DNA-binding abilities [6–8]. This kind of complexes could bind to DNA by intercalating, groove binding and electrostatic modes, and those ones with larger aromatic intercalating ligands often show higher binding abilities [9–11]. For instance, complexes with porphyrin coordinated to two [Ru (bipy)$_2$Cl]$^+$ (bipy = 2,2-bipyridine) groups, could convert plasmid pBR 322 DNA from the supercoiled to the nicked form, and even to the linear form with the presence of light [12]. Ru complexes attached to asymmetric porphyrins, such as [Ru(L)$_2$MPyTPPCl]Cl (L = bpy, phen or pip; bpy = 2,2-bipyridine; phen = 1,10-phenanthroline; pip = 2-Phenyl-1*H*-1,3,7,8-tetraazacyclopenta[*l*]phenanthrene; MPyTPP = 5-(4′-pyridine)-10,15,20-triphenyl porphyrin), exhibited high affinity to nucleic acids,

* Corresponding authors at: Department of Chemistry, College of Life Science and Technology, The Second Science Engineering Building, Jinan University, Guangzhou 510632, PR China. Tel.: +86 20 8522 8321; fax: +86 20 8522 8321.
E-mail addresses: tliuliu@jnu.edu.cn (J. Liu), tzhwj@jnu.edu.cn, yananliu.jl@gmail.com (W.-J. Zheng).

0009-2797/$ – see front matter © 2009 Elsevier Ireland Ltd. All rights reserved.
doi:10.1016/j.cbi.2009.11.026

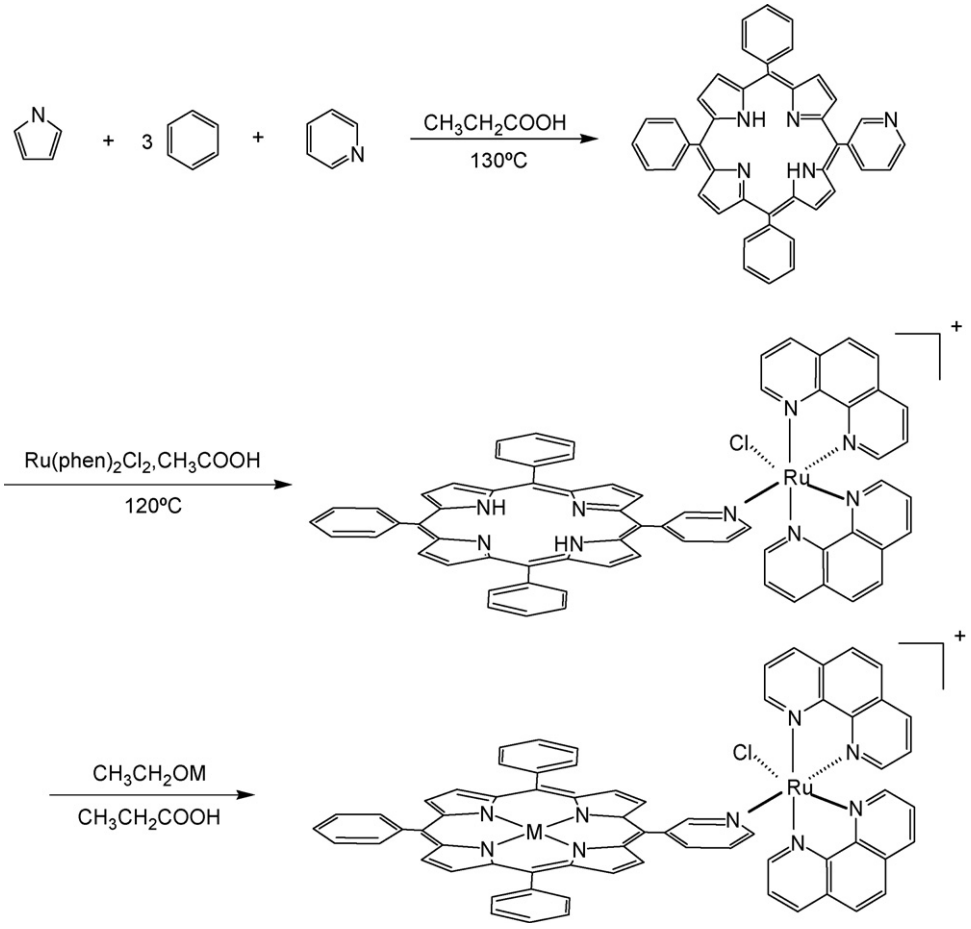

Scheme 1. Schematic routes for synthesis of Ru porphyrin complexes **1** (M = 2H); **2** (M = Ni); **3** (M = Cu).

including calf thymus DNA (CT-DNA), RNA and G-quadruplex, indicating that this type of complexes has potential in chemotherapy [13–15].

However, studies also reported that the DNA-binding abilities of Ru complexes were not positively related to their antitumor activities. One of the reasons should be their difference in the solubility, which may affect their effective crossing of the cell membrane [16]. Thus, during the past years, a lot of potent Ru porphyrin complexes have been designed to achieve better solubility and greater chemopreventive efficacy by structural modifications. Studies have revealed that the antitumor activity of Ru complexes can be significantly improved by introducing hydrophobic porphyrin molecules [17–19]. For example, increase in lipid/water partition and membrane binding has been found in Ru complexes with cationic porphyrin groups [20]. Schmitt and co-workers have shown that ruthenated porphyrin, $[Ru_4(\eta^6\text{-}C_6H_5CH_3)_4(TPP)Cl_8]$ (TPP = 5,10,15,20-tetra(4-pyrid-yl) porphyrin), could effectively cross the cell membrane and accumulate in the granular structures of melanoma cells [21]. In the present study, the synthesis of a Ru porphyrin complex, [(Py-3′)TPP-Ru(phen)$_2$Cl]Cl ((Py-3′)TPP = 5-(3′-pyridyl-10,15,20-triphenylporphyrin) and its heterometallic derivatives (Scheme 1), and their interaction with CT-DNA were investigated. The photocleavage properties of these complexes against the plasmid PBR 322 DNA were also examined by gel electrophotolysis experiments. Moreover, we screened their antiproliferative and apoptosis-inducing activities and elucidated the molecular mechanisms of apoptotic cell death induced by the complexes in selected cancer cells.

2. Materials and methods

2.1. Materials

Pyrrole (CP, Fluka), benzaldehyde (AR, Fluka) and 3-aldehyde pyridine (AR, Acros) were purchased commercially and used without further purification unless specially noted. Calf thymus DNA (CT-DNA) was purchased from the Sino-American Biotechnology Company and the plasmid DNA, pBR322 DNA, was from the Sangon Biotechnology Company (Canada). DNA Solutions in 5 mM Tris–HCl buffer (pH 7.2), 50 mM NaCl gave a ratio of UV absorbance (260/280 nm) of 1.8–1.9:1, indicating that the DNA was sufficiently free of protein. The concentration of CT-DNA was determined spectrophotometrically by using the molar absorption coefficient of 6600 M^{-1} cm^{-1} (260 nm). Thiazolyl blue tetrazolium bromide (MTT) and propidium iodide (PI) were obtained from Sigma. Dulbecco's modified Eagle's medium (DMEM), RPMI-1640 medium, bovine calf serum, and the antibiotic mixture (penicillin–streptomycin) were purchased from Invitrogen (Carlsbad, CA). Milli-Q water was used to prepare buffer solutions.

2.2. Physical measurements

Elemental analyses for C, H and N were carried out with a PerkinElmer 240C elemental analyser. Electrospray ionisation mass spectra (ESI–MS) were acquired on a Thermo Finnigan LCQ DECA XP ion trap mass spectrometer, equipped with an ESI source. The concentrations of Ru, Ni and Cu were determined by ICP–AES analysis. The compounds (5 mg) were digested with 3 mL concentrated

nitric acid and 1 mL H_2O_2 in a digestive stove (Qian Jian Measuring Instrument Co., China) at 180 °C for 3 h.

Emission spectra of the synthetic Ru porphyrin complex were measured on a Shimadzu RF-5000 fluorescence spectrophotometer with excitation at 459 nm. Electronic spectra were recorded on a Shimadzu UVPC-3000 spectrophotometer. Spectroscopic titrations were carried out under room temperature to determine the binding affinity between DNA and Ru porphyrin complexes. Briefly, 3.0 mL of Tris–HCl buffer (pH 7.2, [NaCl] = 50 mM) was placed in the reference cuvette (1 cm path length) and Ru porphyrin complex samples (20 μM) were added to the sample cuvettes (1 cm path length). Then aliquots (1–10 μL) CT-DNA solution at 3.0 mM in base pairs were added to both of the reference and sample cuvettes. Finally, the spectra were recorded in the range of 200–700 nm and the titration processes were repeated until no further changes in the spectra of four titrations were observed, which suggests that the binding saturation had been achieved. Every experiment was repeated three times at least.

Viscosity measurements were carried out using an Ubbelodhe viscometer maintained at 30.0 ± 0.1 °C in a thermostatic bath. The DNA samples contained approximately 200 base pairs. The flow time was measured with a digital stopwatch and each sample was measured three times. Data are presented as $(\eta/\eta^0)^{1/3}$ vs. binding ratio, where η is the viscosity of DNA in the presence of the complexes and η^0 is the viscosity of DNA in the absence of the complexes.

For the gel electrophotolysis experiments, supercoiled plasmid pBR 322 DNA (10 μM) was treated with the complexes in 50 mM Tris–HCl buffer (pH 8.3, [NaCl] = 18 mM), and then the solutions were irradiated with a UV lamp (254 nm, 10 W) at room temperature for 60 min. The samples were then analyzed by electrophotolysis for 2–3 h at 50 V on 1% agarose gel in Tris–boracic acid–EDTA buffer. The gel was stained with 0.5 μg mL^{-1} ethidium bromide (EB) and photographed under UV light. All experiments were performed at least in triplicate.

2.3. Synthesis and characterizations

The Schematic routes for the synthesis of complexes **1**, **2** and **3** were shown in Scheme 1.

2.3.1. Synthesis of [(Py-3′)TPP]

[(Py-3′)TPP] was synthesized according to the literature [22]. Briefly, a mixture of benzaldehyde (7.5 mL, 0.072 mol) and 3-aldehyde pyridine (2.5 mL, 0.024 mol) in propionic acid (150 mL) was heated until refluxing, then a solution of freshly distilled pyrrole (7.0 mL, 0.11 mol) in propionic acid (100 mL) was added dropwise with vigorous stirring throughout. After refluxing for another 45 min, the mixture was cooled to ambient temperature, and anhydrous alcohol (200 mL) was added. The mixture was kept at −20 °C overnight, and the indigo solid was isolated by suction filtration, washing with alcohol, and drying in vacuum. The products were then purified by silica gel column chromatography with chloroform and alcohol (v/v, 10:1) as eluant. The second purple-red band was collected. The solvents were removed under reduced pressure, and the final products were obtained by recrystallization from chloroform-alcohol. Yield: 0.44 g (2%, calculated to pyrrole).

2.3.2. Synthesis of [(Py-3′)TPP-Ru(phen)$_2$Cl]Cl (**1**)

Compound **1** was synthesized according to the literature [23]. A mixture of [(Py-3′)TPP] (0.062 g, 0.1 mmol), *cis*-Ru(phen)$_2$Cl$_2$ (0.080 g, 0.2 mmol) and acetic acid (10 mL) was stirred and refluxed under argon for 45 min. A dark red solid was obtained on removal of the solvent under decompression evaporation. The product was dissolved in methanol, and refluxed for another 45 min. The complex was precipitated by addition of a saturated acetone solution of LiCl, then filtered off and dried under vacuum. The crude product was separated and purified by column chromatography with chloroform and methanol (v/v, 20:1) as eluant. The second brown-red band was collected, and dried under rotary evaporation, to get a brown solid. Yield: 89% (calculated according to [(Py-3′)TPP]). Found (%): C, 69.91; H, 4.07; N, 11.09; calculated for [$C_{67}H_{45}N_9ClRu$]Cl (%): C, 70.09; H, 3.95; N, 10.98. UV–vis (in CH_3CN, $10^{-4}\varepsilon$ (M^{-1} cm^{-1})): 646.5(0.3), 589.5(0.5), 550.5(0.9), 514.0(1.6), 415.0(14.4) and 266.0 (4.6) nm. ESI-MS: *m/z* 1113 [M−Cl]$^+$.

2.3.3. Synthesis of [Ni(Py-3′)TPP-Ru(phen)$_2$Cl](PF$_6$) (**2**)

A mixture of nickel chloride (50 mg), **1** (50 mg) and acetic acid (10 mL) was stirred for 1 h under ambient temperature. A dark red solid was obtained by suction filtration, washed with ether and dried under vacuum. The product was dissolved in a minimal amount of DMF, then reprecipitated by the addition of a saturated aqueous solution of ammonium hexafluorophosphate. The product was filtered off, washed several times with water and ether, yields, 81%. Found (%): C: 61.03; H: 3.52; N: 9.49; calculated for [$C_{67}H_{43}N_9ClNiRu$]PF_6 (%): C: 61.13; H: 3.45; N: 9.58; UV–vis (in CH_3CN, $10^{-4}\varepsilon$ (M^{-1} cm^{-1})): 538.1(0.9), 414.5(12.3) and 267.1 (3.6) nm. ESI-MS: 1211 [M−$PF_6^+CH_3CN$]$^+$.

2.3.4. Synthesis of [Cu(Py-3′)TPP-Ru(phen)$_2$Cl](PF$_6$) (**3**)

Compound **3** was prepared in a way similar to **2**, but with copper (II) acetate and [Ru(phen)$_2$(P3TPP)Cl]PF_6, yield, 79%. Found (%): C: 60.82; H: 3.52; N: 9.39; calculated for [$C_{67}H_{43}N_9ClCuRu$]PF_6 (%): C: 60.91; H: 3.43; N: 9.54;UV–vis (in CH_3CN, $10^{-4}\varepsilon$ (M^{-1} cm^{-1})): 568.4(1.0), 412.0(14.3) and 266.2 (3.1) nm. ESI–MS: *m/z* 1175 [M−PF_6]$^+$.

2.4. Cell culture

The cell lines used in this study, including A375 human melanoma cells, MCF-7 human breast adrenocarcinoma cells, Colo201 human colon adenocarcinoma cells and Hep G2 human liver cancer cells, were obtained from American Type Culture Collection (Manassas, VA). Cells were maintained in either DMEM (for A375 cells) or RPMI 1640 (for MCF-7, Colo201 and Hep G2 cells) medium supplemented with 10% fetal bovine serum, penicillin (100 units/mL) and streptomycin (50 units/mL) at 37 °C in a humidified incubator with 5% CO_2 atmosphere.

2.5. MTT assay

Cell viability was determined by measuring the ability of the cells to transform MTT to a purple formazan dye [24]. Cells were seeded in 96-well tissue culture plates at 2.5×10^3 cells/well for 24 h. The cells were then incubated with the test compounds at different concentrations for 48 h. After incubation, 20 μL/well of MTT solution (5 mg/mL phosphate buffered saline) was added and incubated for 5 h. The medium was aspirated and replaced with 150 μL/well DMSO to dissolve the formazan salt. The color intensity of the formazan solution, which reflects the cell growth condition, was measured at 570 nm using a microplate spectrophotometer (SpectroAmax^{TM} 250).

2.6. Flow cytometric analysis

Flow cytometric analysis was carried out according to our previous method [25]. Briefly, cells exposed to the complexes were harvested by centrifugation and washed with PBS. Cells were stained with PI after fixation with 70% ethanol at −20 °C overnight. The DNA content was analyzed with a Beckman Coulter Epics XL MCL flow cytometer (Miami, FL). The cell cycle distribution was analyzed using MultiCycle software (Phoenix Flow Systems,

San Diego, CA). The proportions of cells in G0/G1, S, and G2/M phases were represented as DNA histograms. Apoptotic cells with hypodiploid DNA contents were measured by quantifying the sub-G1 peak. For each experiment, 10,000 events per sample were recorded.

2.7. Evaluation of mitochondrial membrane potential ($\Delta\Psi_m$)

Cells in 6-well plates were trypsinized and resuspended in 0.5 mL of PBS buffer containing 10 μg/mL of JC-1. After incubation for 10 min at 37 °C in the incubator, cells were immediately centrifuged to remove the supernatant. Cell pellets were suspended in PBS and then analyzed by flow cytometry. The percentage of the green fluorescence from JC-1 monomers was used to represent the cells that lost $\Delta\Psi_m$.

2.8. Western blot analysis

Whole cellular proteins were extracted by incubation the cell pellets with cell lysis buffer (Cell Signaling Technology) overnight at 4 °C. Protein concentration was determined by bicinchoninic acid assay (Sigma) according to the manufacturer's instructions. SDS-PAGE was done in 10% tricine gels loading 40 mg of cell lysates per lane. After electrophoresis, separated proteins were transferred to nitrocellulose membrane and blocked with 5% non-fat milk in TBST buffer for 1 h. After then, the membranes were incubated with primary antibodies at 1:1000 dilutions in 5% non-fat milk overnight at 4 °C with continuous agitation, and then secondary antibodies conjugated with horseradish peroxidase at 1:2000 dilution for 1 h at room temperature. Protein bands were visualized on X-ray film using an enhanced chemiluminescence system (Kodak).

2.9. Statistical analysis

Experiments were carried out at least in triplicate and results were expressed as mean ± S.D. Statistical analysis was performed using SPSS statistical program version 13 (SPSS Inc., Chicago, IL). Difference with $p < 0.05$ (*) or $p < 0.01$ (**) was considered statistically significant.

3. Results and discussion

3.1. DNA-binding properties of the synthetic Ru porphyrin complexes

Spectrophotometry is the most common method to investigate the interaction of transition metal complexes with DNA. In general, transition metal complexes exhibit hypochromism and red shift in their electronic spectra when they are bound to DNA. The degree of hypochromism depends on the binding mode and affinity. The changes in the electronic spectra of complexes **1**, **2** and **3** in the absence or presence of CT-DNA were showed in Fig. 1. In Tris–HCl buffer (pH 7.2), all these complexes exhibited strong absorptions in the electronic spectra. For complex **1**, there were characteristic intraligand (IL) transition and Soret absorptions at 267 and 406 nm, respectively. The characteristic Q-band absorptions attributed to the porphyrin ring were present at 521, 558, 594 and 650 nm. For complex **2**, the characteristic IL and Soret absorptions appeared at 268 and 406 nm, respectively, with the Q bands at 543 and 587 nm. For complex **3**, the IL and Soret absorptions were at 267 and 406 nm, respectively, with the Q band at 568 nm. These data were consistent with those reported in the literature [26].

As listed in Table 1, when CT-DNA was added to the complexes, obvious hypochromism and red shift in both the IL and Soret absorptions were observed in all complexes. The hypochromism and red shift for **1** were larger than those of **2** and **3**, indicating that

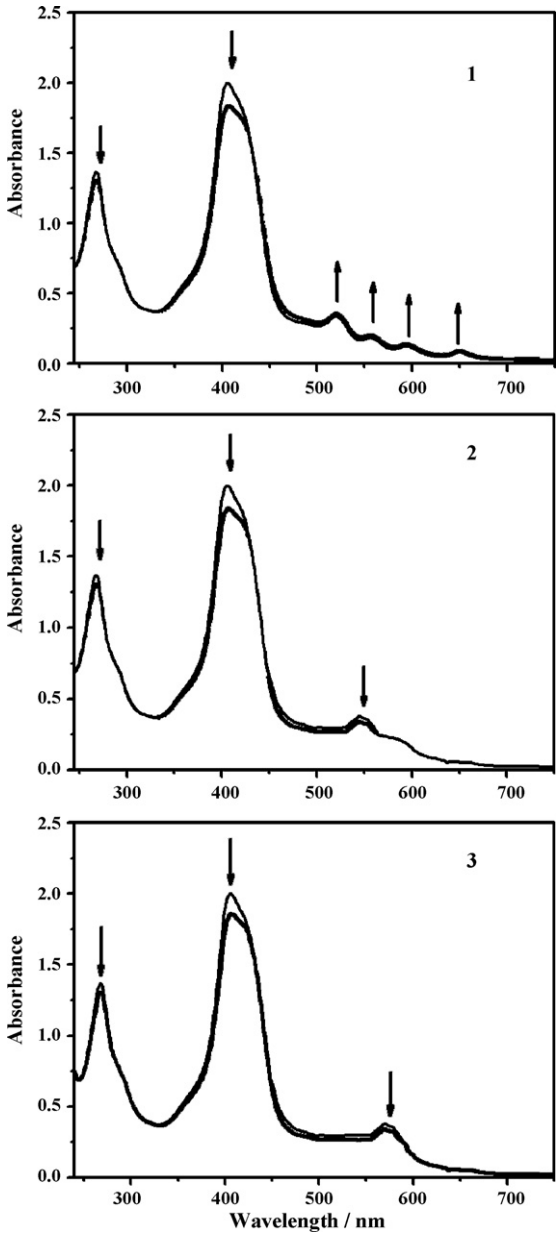

Fig. 1. Absorption spectra of complexes **1**, **2** and **3** in 5 mM Tris buffer, pH 7.2 in the absence and presence of calf thymus DNA. [Ru] = 20.0 μM, [DNA] = 54 μM.

the binding affinity of **1** was higher than those of **2** and **3**. To further clarify the DNA-binding behavior of these complexes, the intrinsic binding constants (K_b) were calculated according to the decay of the Soret absorption by Eq. (1) [27].

$$\frac{(\varepsilon_a - \varepsilon_f)}{(\varepsilon_b - \varepsilon_f)} = \frac{(b - (b^2 - 2K_b^2 C_t[\mathrm{DNA}]/s)^{1/2})}{2K_b C_t} \quad (1a)$$

$$b = 1 + K_b C_t + \frac{K_b[\mathrm{DNA}]}{2s} \quad (1b)$$

where [DNA] is the concentration of DNA in nucleotides, while the ε_a, ε_f and ε_b are the apparent extinction coefficient (A_{abs}/[M]), the extinction coefficient for free metal complex (M) and the metal complex in the fully bound form, respectively. K_b is the equilibrium binding constant in M^{-1}. Ct is the total Ru(II) complex concentration and s is the binding-site size. Values of ε_b were obtained by extrapolation from the y intercept of plots of $\varepsilon_a/\varepsilon_f$ vs. 1/[DNA]. The K_b and s values are those for the best least-squares fits to

Table 1
Changes in electronic spectra of complexes **1**, **2** and **3** in the absence or presence of CT-DNA in 5 mM Tris–HCl buffer, 0.1 mM NaCl (pH 7.2).

Complex	λ_{max} (free)	λ_{max} (bound)	$\Delta\lambda$ (nm)	H (%)	K_b (M^{-1})
1	405	407	2	11	1.35×10^5
	267	267	0	4	
2	406	407	1	8	1.29×10^5
	267	267	0	2	
3	405	406	1	7	1.22×10^5
	267	27	0	2	

the individual UV/vis titration curves using the program ORIGIN 6.0. In the present study, the calculated intrinsic binding constants (K_b) for complexes **1**, **2** and **3** were $(1.35 \pm 0.5) \times 10^5\ M^{-1}$ ($s = 4.2$), $(1.29 \pm 0.5) \times 10^5\ M^{-1}$ ($s = 5.6$) and $(1.22 \pm 0.5) \times 10^5\ M^{-1}$ ($s = 6.2$), respectively. Therefore, the DNA-binding constants of complexes follow the order of K_b (**1**) > K_b(**2**) > K_b(**3**), indicating that the binding affinity (A) of complexes is in the order of A(**1**) > A(**2**) > A(**3**).

3.2. EB-quenching properties of the complexes

Complexes **1**, **2** and **3** alone exhibited only weak fluorescence in the presence or absence of CT-DNA, thus EB-quenching experiments were carried out to further characterize the binding of these complexes to DNA. EB emits intense fluorescence in the presence of DNA, due to its strong intercalation between the base pairs, which can be quenched by competition between the complexes and EB for binding to DNA. Previous studies have showed that the fluorescence quenching of EB–DNA by tetraazza marocyclic complexes could be due to the replacement of the DNA intercalator [23]. In this study, as shown in Fig. 2, the fluorescence intensity of EB decreased gradually in the presence of the complexes, indicating that the EB molecules were being displaced from the DNA helix by the complex molecules. The quenching constant K_q of each complex was calculated according to the classical Stern–Volmer equation [28]:

$$\frac{I_0}{I} = 1 + K_q r \quad (2)$$

where I_0 and I are the fluorescence intensities in the absence or presence of the complexes, and r is the ratio of [Ru]/[DNA]. K_q is a linear Stern–Volmer quenching constant depending on the ratio of EB to DNA. In this study, the quenching constants K_q for **1**, **2** and **3** according to the decay of EB fluorescence were 18.8, 17.7 and 15.8, respectively. These data indicate that the binding affinity of these complexes was in the sequence of complex **1** > complex **2** > complex **3**, which was consistent with the changes in the electronic absorption spectra.

3.3. Viscosity measurements

In general, the viscosity of double strand DNA would increase when a complex binds to DNA in intercalating mode, but remain unchanged when a complex binds to DNA in electrostatic mode. For those complexes binding to DNA in the groove binding mode, the viscosity of DNA will decrease since the DNA helix will be bent [29,30]. The changes in the viscosity of DNA in the presence of the complexes were shown in Fig. 3. The relative viscosity of CT-DNA decreased in the presence of all three complexes, indicating that these complexes may bind to DNA through groove binding mode (Fig. 3). Furthermore, the decrease for complex **1** was more significant than those of **2** and **3**, indicating that the affinity of **1** to DNA was the strongest among the three complexes, which was also in agreement with the spectroscopic results.

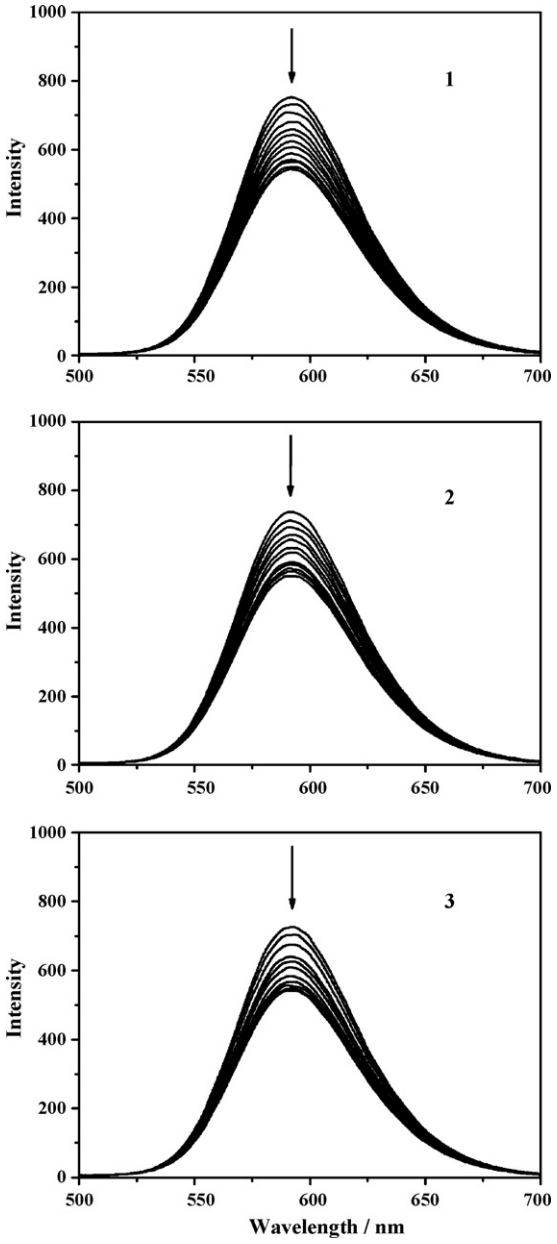

Fig. 2. Changes in fluorescence of EB in presence of complexes **1**, **2** and **3**. [EB] = 4 μM, [DNA] = 100 μM.

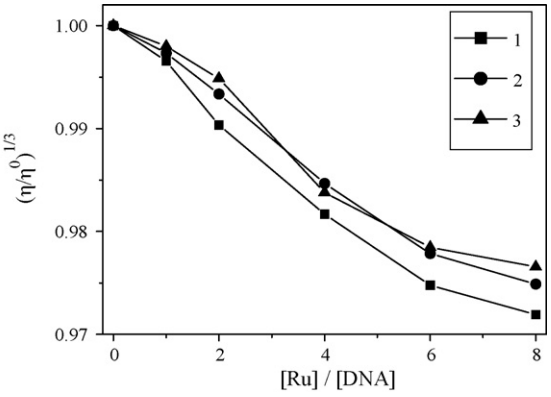

Fig. 3. Effects of complexes **1**, **2** and **3** on the relative viscosities of CT-DNA at 30.0 °C (±0.1 °C), [DNA] = 500 μM.

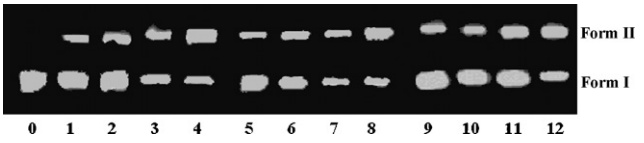

Fig. 4. Photocleavage of pBR 322 DNA with the absence (Lane 0) or presence of complexes **1** (Lanes 1–4), **2** (Lanes 5–8) and **3** (Lanes 9–12). The concentrations of these complexes were 15 (Lanes 1, 5 and 9), 30 (Lanes 2, 6 and 10), 45 (Lanes 3, 7 and 11) and 60 μM (Lanes 4, 8 and 12), respectively.

Table 2
Growth inhibition of Ru porphyrin complexes on various human cancer cells.

Complex	IC_{50} (μg/mL)			
	A375	Hep G2	Colo201	PC-3
1	4.4 ± 0.9	8.7 ± 1.3	16.8 ± 1.9	25.1 ± 3.4
2	9.7 ± 1.1	11.2 ± 0.7	18.6 ± 2.4	32.7 ± 4.1
3	12.7 ± 1.8	25.6 ± 3.9	47.6 ± 3.6	74.2 ± 6.5

Cells were treated with various concentrations of tested compounds for 48 h. Cell viability was determined by MTT assay and IC50 values were calculated as described in the Experimental section. Each value represents the mean ± S.D. of three independent experiments.

3.4. Photocleavage of pBR 322 DNA by Ru porphyrin complexes

The gel electrophoretic separation showing the cleavage of plasmid pBR322 DNA induced by the complexes under identical conditions is shown in Fig. 4. It can be seen that only supercoiled form (Form I) of pBR 322 DNA was observed in control group (Lane 0). However, all the tested Ru porphyrin complexes could cleave pBR 322 DNA from supercoiled form to nicked circular form (Form II) in a dose-dependent manner, and the activity followed the order **1** > **2** > **3**, which was consistent with that observed in the above measurements. These results indicated that cleavage of single chain DNA occurred, and the DNA molecules were then converted from supercoiled form to nicked form.

3.5. Apoptosis-inducing activities of Ru complexes and the underlying mechanisms

The antiproliferative activities of the complexes were first screened by MTT assay against a panel of four human cancer cell lines, including A375 human melanoma cells, MCF-7 human breast adrenocarcinoma cells, Colo201 human colon adenocarcinoma cells and Hep G2 human liver cancer cells. As shown in Table 2, the complexes exhibited broad inhibition on the four tested human cancer cell lines, with IC_{50} values ranging from 4.4 to 74.2 μM. The lower IC_{50} values of complex **1** as compared with the other tested complexes, indicates its higher cytotoxic effects against human cancer cells. The *in vitro* anticancer activities of these complexes was in the sequence of complex **1** > complex **2** > complex **3**, which was consistent with the trends of their DNA-binding and photocleavage abilities.

Inhibition of cancer cell proliferation by cytotoxic drugs could be the result of induction of apoptosis or of cell cycle arrest, or a combination of these two modes [24,25]. According to the results of broad screening (Table 2), A375 cells exhibited the highest sensitivity to complex **1**. Thus this cell line was used for further investigation on the underlying mechanisms accounting for the antiproliferative action of complex **1**. Flow cytometric analysis was carried out to determine the possible mechanisms of cell growth inhibition. Fig. 5 shows the representative DNA distribution histograms of A375 cells incubated in the absence or presence of 5, 10 and 20 μg/mL complex **1** for 48 h. Exposure of A375 cells to complex **1** led to marked dose-dependent increases in the proportion of apoptotic cells, as reflected by the sub-diploid peaks. Moreover, treatment with complex **1** caused a slight increase in the percentage of cells at G0/G1 phase, accompanied by a corresponding reduction in the percentage of cells at d G2/M phase, indicating the induction of G0/G1-phase arrest by complex **1**. Previous studies have suggested that many antitumor agents used in chemotherapy are based on their apoptosis-inducing effects and cytostatic activities on cancer cells [31]. Our results indicate that Ru porphyrin complex **1** is a promising novel synthetic compound with potential in treatment of cancers.

3.6. Mitochondria plans an important role in Ru complexe-induced apoptosis

Mitochondria act as a point of integration for apoptotic signals originating from both the extrinsic and intrinsic apoptotic pathways [32]. Loss of $\Delta\Psi_m$ is associated with the activation of caspases and the initiation of apoptotic cascades. Thus, the status of mitochondria in A375 cells exposed to complex **1** was investigated by JC-1 flow cytometric analysis. In this study, it was found that complex **1** induced significant depletion of $\Delta\Psi_m$ in A375 cells (Fig. 6A). The percentage of cells with depolarized mitochondria increased from 6.86% (control) to 15.99% (5 μM), 28.83% (10 μM) and 42.22% (20 μM), respectively. These results indicated that complex **1** induced apoptosis in A375 cells through mitochondria-mediated pathways.

The mitochondria-mediated apoptosis is precisely regulated by the proteins that comprise a large group termed the Bcl-2 family [33]. Pro-survival family members associate with the mitochondrial outer membrane and maintain their integrity. In contrast, pro-apoptotic members such as Bax and Bak oligomerize in mitochondrial outer membrane and disrupt their integrity, causing the release of apoptogenic factors [33]. By western blot analysis, we observed that complex **1** up-regulated the expression of Bax, but

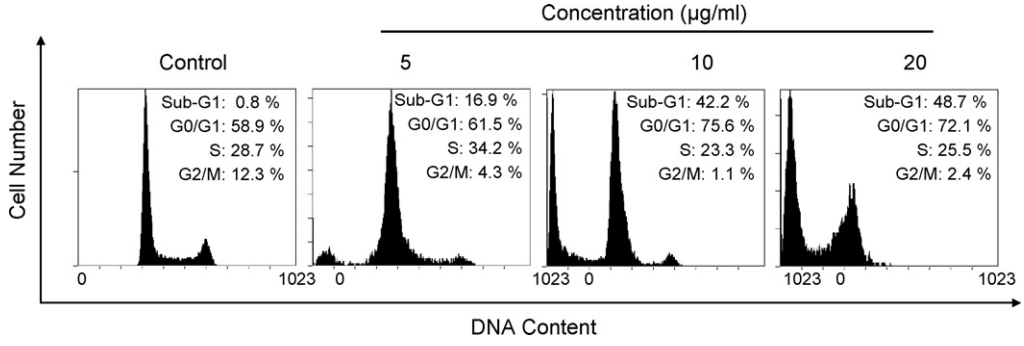

Fig. 5. Effects of complex **1** on cell apoptosis and cell cycle distribution in A375 human melanoma cells. The cells treated with different concentrations of Ru porphyrin complex **1** for 48 h were collected and stained with PI after fixation as described in the Experimental section. Cellular DNA histograms were analyzed by the MultiCycle software. Each value represents the mean of three independent experiments.

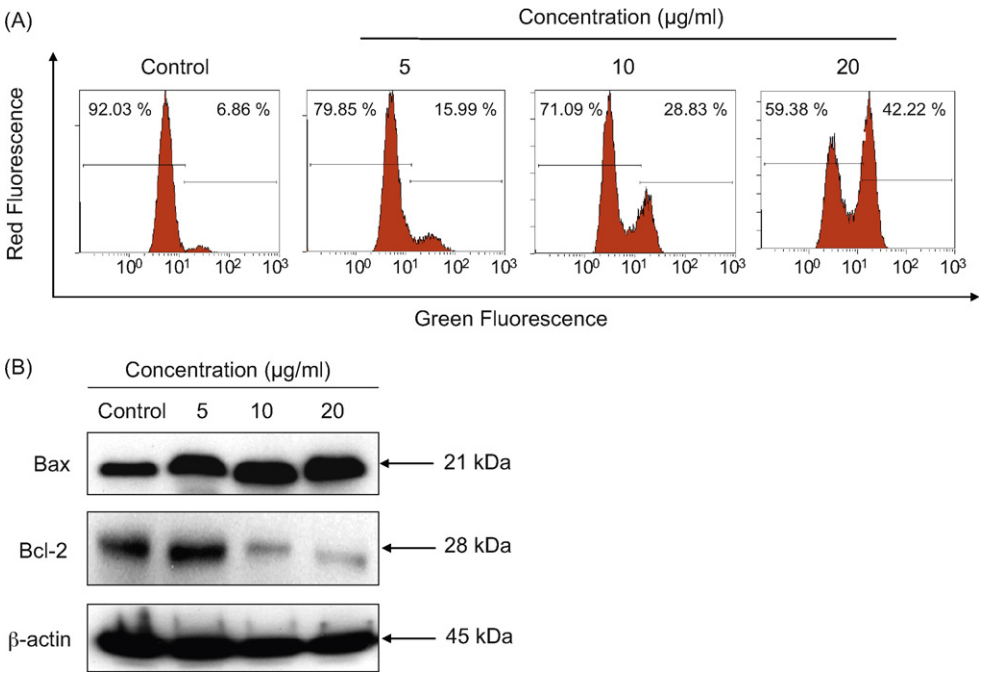

Fig. 6. Complex **1** induces the depletion of mitochondrial membrane potential ($\Delta\Psi_m$) and regulates the expression of Bcl-2 and Bax proteins in A375 cells. (A) Cells treated with complex **1** were harvested and stained with the mitochondria-selective dye JC-1 and then analyzed by flow cytometry. The number in the right region of each dot plot represents the percentage of cells that emit green fluorescence due to the depletion of $\Delta\Psi_m$. (B) Regulation of Bcl-2 and Bax expression by complex **1** in A375 cells. Cells were treated with 10, 20 and 40 mM of complex **1** for 24 h. All experiments were carried out at least in triplicates.

down-regulated the expression of Bcl-2 (Fig. 6B). These results support that complex **1** induces mitochondria-mediated apoptosis by regulating the expression of Bcl-2 family proteins.

4. Conclusion

The binding behaviors of Ru porphyrin complexes to calf thymus DNA were subtly but distinctly different, depending on their chemical structures. All three synthetic Ru porphyrin complexes bound to DNA by groove binding mode and the DNA-binding constants (K_b) were in order of $K_b(\mathbf{1}) > K_b(\mathbf{2}) > K_b(\mathbf{3})$, indicating that the presence of the Ni and Cu ions had no effect on the binding mode, but reduced the binding affinity of these complexes. Ru porphyrin complexes could cleave supercoiled DNA to single chain DNA, indicating their novel photocleavage properties. Moreover, these complexes were also identified as potent antiproliferative agents against A375 human melanoma cells, MCF-7 human breast adenocarcinoma cells, Colo201 human colon adenocarcinoma cells and Hep G2 human liver cancer cells. Complex **1** inhibits the growth of A375 cells through induction of apoptotic cell death and G0/G1 cell cycle arrest. Further investigation showed that complex **1** induces mitochondria-mediated apoptosis by regulating the expression of Bcl-2 family proteins. Our results suggest that ruthenium porphyrin complexes could be a candidate for further evaluation as a chemopreventive and chemotherapeutic agent for human cancers.

Conflict of interest

None declared.

Acknowledgements

This work was supported by the National Natural Science Foundation of China (20871056, 20771044, 20901030), the Natural Science Foundation of Guangdong Province (8251063201000008, 9451063201002077), the Planned Item of Science and Technology of Guangdong Province (2008A030201020), and the 211 project grant of Jinan University.

References

[1] C.M. Che, J.Sh. Huang, Ruthenium and osmium porphyrin carbene complexes: synthesis, structure, and connection to the metal-mediated cyclopropanation of alkenes, Coord. Chem. Rev. 231 (1–2) (2002) 151–164.
[2] M.R. Maurya, L.K. Woo, Metalloporphyrin as a ligand in organometallic complexes: Synthesis and characterization of a nickel (II) porphyrin complex of 1,5-cyclooctadienedichlororuthenium (II), J. Organomet. Chem. 690 (21–22) (2005) 4978–4981.
[3] D.L. Ma, C.M. Che, S.C. Yan, Platinum(II) complexes with dipyridophenazine ligands as human telomerase inhibitors and luminescent probes for G-quadruplex DNA, J. Am. Chem. Soc. 131 (5) (2009) 1835–1846.
[4] E.Z. Moreira, L.A.B.d. Moraes, M.N. Eberlin, Y. Iamamoto, S. Nikolaou, The use of electrospray ionization tandem mass spectrometry on the structural characterization of novel asymmetric metallo-organic supermolecules, based on pentafluorophenylporphyrins and ruthenium complexes, Polyhedron 27 (12) (2008) 2721–2729.
[5] D.J. Vinyard, S. Swavey, M.M. Richter, Photoluminescence and electrogenerated chemiluminescence of a bis(bipyridyl)ruthenium(II)–porphyrin complex, Inorg. Chim. Acta 360 (5) (2007) 1529–1534.
[6] D. Miyoshi, M. Inoue, N. Sugimoto, DNA logic gates based on structural polymorphism of telomere DNA molecules responding to chemical input signals, Angew. Chem. Int. Ed. 45 (46) (2006) 7716–7719.
[7] L.M. Chen, J. Liu, J.C. Chen, S. Shi, C.P. Tan, K.Ch. Zheng, L.N. Ji, Experimental and theoretical studies on the DNA-binding and spectral properties of water-soluble complex $[Ru(MeIm)_4(dpq)]^{2+}$, J. Mol. Struct. 881 (1–3) (2008) 156–166.
[8] J. Liu, W.J. Zheng, S. Shi, C.P. Tan, J.C. Chen, K.Ch. Zheng, L.N. Ji, Synthesis antitumor activity and structure–activity relationships of a series of Ru (II) complexes, J. Inorg. Biochem. 102 (2) (2008) 193–202.
[9] P.K.L. Fu, P.M. Bradley, C. Turro, Stabilization of duplex DNA structure and suppression of transcription in vitro by bis(quinone diimine) complexes of Rh(III) and Ru (II), Inorg. Chem. 43 (6) (2004) 2220–12220.
[10] S. Shi, J. Liu, J. Li, K.Ch. Zheng, X.M. Huang, C.P. Tan, L.M. Chen, L.N. Ji, Synthesis, characterization and DNA-binding of novel chiral complexes D- and K-$[Ru(bpy)_2L]^{2+}$ (L = o-mopip and p-mopip), J. Inorg. Biochem. 100 (3) (2006) 385–395.
[11] S. Basu, S. Halder, I. Pal, S. Samanta, P. Karmakar, M.G.B. Drew, S. Bhattacharya, 1-(2′-Pyridylazo)-2-naphtholate complexes of ruthenium: synthesis, characterization, and DNA binding properties, Polyhedron 27 (13) (2008) 2943–2951.
[12] M. Narra, P. Elliott, S. Swavey, Synthesis, characterization and DNA interactions of 5,15-(4-pyridyl)-10,20-(pentafluorophenyl) porphyrin coordinated to two $[Ru(bipy)_2Cl]^+$ groups, Inorg. Chim. Acta 359 (7) (2006) 2256–2262.

[13] S. Shi, J. Liu, T.M. Yao, X.T. Geng, L.F. Jiang, Q.Y. Yang, L. Cheng, L.N. Ji, Promoting the formation and stabilization of G-quadruplex by dinuclear RuII complex $Ru_2(obip)L_4$, Inorg. Chem. 47 (8) (2008) 2910–2912.
[14] I.M. Dixon, F. Lopez, A.M. Tejera, J.P. Este've, M.A. Blasco, G. Pratviel, B. Meunier, A G-quadruplex ligand with 10000-fold selectivity over duplex DNA, J. Am. Chem. Soc. 129 (6) (2007) 1502–1503.
[15] H. Mita, T. Ohyama, Y. Tanaka, Y. Yamamoto, Formation of a complex of 5,10,15,20-tetrakis (N-methylpyridinium-4-yl)-21H,23H-porphyrin with G-quadruplex DNA, Biochemistry 45 (22) (2006) 6765–6772.
[16] J. Sun, S. Wu, Y. An, J. Liu, F. Gao, L.N. Ji, Z.W. Mao, Synthesis, crystal structure and DNA-binding properties of ruthenium (II) polypyridyl complexes with dicationic 2,20-dipyridyl derivatives as ligands, Polyhedron 27 (13) (2008) 2845–2850.
[17] L.L. Jin, T. Chang, H.W. Jing, Coupling of epoxides with carbon dioxide catalyzed by ruthenium porphyrin complex, Chin. J. Catal. 28 (4) (2007) 287–288.
[18] X. Liu, J.H. Liu, K. Jin, X.C. Yang, Q.J. Peng, L.C. Sun, Synthesis, characterization and some properties of amide-linked porphyrin–ruthenium (II) tris (bipyridine) complexes, Tetrahedron 61 (23) (2005) 5655–5662.
[19] B. Serli, E. Zangrando, E. Iengo, E. Alessio, Novel mono- and dinuclear ruthenium nitrosyls with coordinated pyrazine, Inorg. Chim. Acta 339 (1) (2002) 265–272.
[20] F.M. Engelmann, S.V.O. Rocha, H.E. Toma, K. Araki, M.S. Baptisa, Determination of n-octanol/water partition and membrane binding of cationic porphyrins, Int. J. Pharm. 329 (1–2) (2007) 12–18.
[21] F. Schmitt, P. Govindaswamy, G. Süss-Fink, W.H. Ang, P.J. Dyson, L. Juilleratt-Jeanneret, B. Therrien, Ruthenium porphyrin compounds for photodynamic therapy of cancer, J. Med. Chem. 51 (6) (2008) 1811–1816.
[22] E.B. Fleischer, A.M. Shachter, Effect of wall conductivity on thermal stratification, Solar Energy 49 (1992) 273–277.
[23] E.B. Fleischer, A.M. Shachter, Coordination oligomers and a coordination polymer of zinc tetraarylporphyrins, Inorg. Chem. 30 (19) (1991) 3763–3769.
[24] T. Chen, Y.S. Wong, Selenocystine induces S-phase arrest and apoptosis in human breast adenocarcinoma MCF-7 cells by modulating ERK and Akt phosphorylation, J. Agric. Food Chem. 56 (22) (2008) 10574–10581.
[25] T. Chen, Y.S. Wong, Selenocystine induces apoptosis of A375 human melanoma cells by activating ROS-mediated mitochondrial pathway and p53 phosphorylation, Cell Mol. Life Sci. 65 (17) (2008) 2763–2775.
[26] W.J. Mei, Y.X. Liu, Synthesis, characterization and DNA-binding properties of mixed porphyrin–polypyridyl ruthenium (II) complexes, Transit, Met. Chem. 30 (2005) 82–88.
[27] R.P. Hertzberg, P.B. Dervan, Cleavage of double helical DNA by methidium-propyl-EDTA-iron (II), J. Am. Chem. Soc. 104 (1) (1982) 313–315.
[28] A. Czarny, D.W. Boykin, A.A. Wood, C.M. Nunn, S. Neidle, M. Zhao, W.D. Wilson, Analysis of van der Waals and electrostatic contributions in the interactions of minor groove binding benzimidazoles with DNA, J. Am. Chem. Soc. 117 (16) (1995) 4716–4717.
[29] S. Satyanarayana, J.C. Dabroniak, J.B. Chaires, Neither Δ-nor Λ-tris (phenanthroline) ruthenium (II) binds to DNA by classical intercalation, Biochemistry 31 (39) (1992) 9319–9324.
[30] S. Satyanarayana, J.C. Daborusak, J.B. Chaires, Tris (phenanthroline) ruthenium (II) enantiomer interactions with DNA: mode and specificity of binding, Biochemistry 32 (10) (1993) 2573–2584.
[31] R. Kim, Recent advances in understanding the cell death pathways activated by anticancer therapy, Cancer 103 (8) (2005) 1551–1560.
[32] M.V. Gurp, N. Festjens, G.V. Loo, X. Saelens, P. Vandenabeele, Mitochondrial intermembrane proteins in cell death, Biochem. Biophys. Res. Commun. 304 (3) (2003) 487–497.
[33] S. Cory, J.M. Adams, The Bcl-2 family: regulators of the cellular life-ordeath switch, Nat. Rev. Cancer 2 (9) (2002) 647–656.